Supporting Information

Miller et al. 10.1073/pnas.1004704107

SI Text

Experiment-Based Aβ_{1-42} Fibril Models Construction. Recently, based on cryoEM measurements Zhang et al. (1) suggested that Aβ_{42} fibrils can have a *tubular*-like shape with a hollow core. They further proposed that Aβ_{42} modeled based on the Aβ_{17-42} coordinates [derived from hydrogen/deuterium-exchange NMR data, side-chain packing constraints, ssNMR, and EM (PDB ID code 2BEG)] (2) can be arranged to fit the *tubular* density obtained from the cryoEM density map. To fit the structure of Aβ_{42} into the high resolution density map, two different structural models of Aβ based on ssNMR may be used: First is the Lührs model (2) for Aβ_{42} and the second is Tycko's model (3) for Aβ_{40}. When attempting to fit each of these two models into the cryoEM density map, only the dimensions of the Lührs model presented a good fit. Considering these cryoEM (1) density maps and using these NMR-based coordinates of Aβ_{17-42} (2) we then constructed ten 24-mer *tubular* polymorphic models (Fig. 1 and Figs. S1–S3): two 12-mer oligomers in a parallel arrangement.

We used the third monomer conformation of the Aβ_{17-42} peptide from the Aβ pentamer in the PDB coordinate file and generated two 12-mers oligomers in a parallel arrangement. We then linked the L17 of each monomer to the N-terminal fragment peptide (D1-K16), which is not included in the coordinate file because it is disordered in the NMR study. The two 12-mers were joined via the N termini of each peptide from one 12-mer to the loop regions of the other 12-mer.

Overall, in the "classical" Aβ fibril, the orientation of F4 is as constructed in model M1. In the other models, we flipped the N-terminal segments in order to form hydrophobic, charge-charge and side-chain interactions between the N-terminal and the loop region.

Populations and Relative Stabilities for Aβ_{42} Tubular Models Are Affected by pH. Polymorphic behavior may also be seen by comparing the intermolecular interactions between the two 12-mers in the fibril at different pH values. For example at pH = 7, the interactions between the C termini of $M3_1$ and $M4_1$ are similar, whereas the N-termini-loop regions' interactions differ, even though $M3_1$ and $M4_1$ have similar populations and energy values. Similarly, $M3_{2a}$ and $M3_{2b}$ at pH = 5–6 and $M9_3$ and $M10_3$ at pH = 3–4 demonstrate similar populations and energy values. Interestingly, at pH = 5–6, $M2_{2b}$ and $M5_2$ have similar populations and energy values; however, $M2_{2b}$ has hydrophobic interactions between the C termini that face inside the collapsed hollow core, whereas $M5_2$ has hydrophobic interactions in the N-termini-loop regions' domains. Finally, at acidic pH, hydrophobic interactions between the C termini that face inside the hollow core are formed in models that derived from M2, M3, and M4 that do not fit the EM density map. These interactions stabilize the fibril, as seen in the energy values at pH = 5–6 compared to pH = 7. At more acidic pH (pH = 3–4), these models lose the N-termini-loop regions' interactions and therefore are relatively less stable than the models at pH = 5–6.

Molecular Dynamics Simulations Procedure. MD simulations of solvated Aβ_{42} oligomers were performed in NPT (N, number of particles; P, pressure; and T, temperature) ensemble using the NAMD program (4) with the CHARMM27 force field (5, 6) for 60 ns. The oligomers were explicitly solvated with TIP3P water molecules (7, 8). The Langevin piston method (4, 9, 10) with a decay period of 100 fs and a damping time of 50 fs was used to maintain a constant pressure of 1 atm. The temperature (300 K) was controlled by Langevin thermostat with a damping coefficient of 10 ps^{-1} (4). The short-range van der Waals interactions were calculated using the switching function, with a twin range cutoff of 10.0 and 12.0 Å. Long-range electrostatic interactions were calculated using the particle mesh Ewald method with a cutoff of 12.0 Å for all simulations (11, 12). The equations of motion were integrated using the leapfrog integrator with a step of 2 fs. All initial Aβ_{42} oligomers were energy minimized and then solvated in a TIP3P water box with a minimum distance of 15 Å from any edge of the box to any Aβ atom. Any water molecule within 2.5 Å of the Aβ was removed. Counterions (Na^+) were added at random locations to neutralize the Aβ_{42} charge.

The solvated systems were energy minimized for 2,000 conjugated gradient steps, where the distance between the β-sheets in Aβ_{42} is fixed in the range 2.2–2.5 Å. The counterions and water molecules were allowed to move. The hydrogen atoms were constrained to the equilibrium bond using the SHAKE algorithm (13). The minimized solvated systems were heated at 200 K, where all atoms were allowed to move. Then, the systems were heated from 200 K to 250 K for 300 ps and equilibrated at 300 K for 300 ps. At the beginning of the simulations geometrical constraints were performed for each Aβ_{42} oligomer. Table S2 summarizes the geometrical constraints for each Aβ_{42} model. All simulations ran for 60 ns and structures were saved every 10 ps for analysis. These conditions (300 K and 60 ns of time scales) are applied to test the stabilities of all Aβ_{42} oligomers.

The Protein Nanoscale Architecture by Symmetry (PNAS) Program. PNAS is an integrated computational graphics tool written in f90 with OpenGL and Qt GUI running on Linux platform. The goal of PNAS is to create a representative atomic model for any protein nanostructure that can be built from identical repetitive units. Similar to a repetitious 3D unit cell that constitutes a single crystal, a 1D line unit or a 2D unit cell (when repetitively transformed by specified symmetry operations) can create a nanostructure such as helical fibril (or tube), spherical cage, and cylindrical tubule. In addition to the capability of creating a structure from scratch via interactive graphic operations, the PNAS also can perform real-time structural optimization, as well as molecular dynamics simulation on the constructed atomic model using molecular mechanics force field such as CHARMM22. Furthermore, to validate an object constructed in silico, the PNAS computes a variety of simulated properties that may be compared with the experimental measurements such as cryoEM map, powder diffraction, and fiber diffraction.

Simulated EM Map. Similar to experimental cryoEM density map, the simulated electron density map is calculated in terms of a set of grid points (voxels). The calculated electron density at each grid point is a sum of electron density contributed from each atom in the model structure. In the PNAS program, the atomic electron density is represented by a Gaussian function. The simulated electron density map, for a set of N atoms, is calculated using the following equation:

$$\rho(i,j,k) = \sum_{n=1}^{N} Z_n \exp\left[1 - \frac{3}{2\sigma^2}\{(x_i - x_n)^2 + (y_j - y_n)^2 + (z_k - z_n)^2\}\right],$$

where (i, j, k) denotes a given grid point (x_i, y_j, z_k) and Z_n is the atomic number of atom (x_n, y_n, z_n), which represents the number of electrons in the atom n. The cutoff distance from the grid point is 3σ. The resolution of a simulated map is equal to 2σ (14).

The isosurface generation of a grid-point EM map is done by the marching cubes algorithm (15). Either an experimental or simulated EM map, a value of 33% of the maximum positive voxel was set to draw the isosurface.

Generalized Born Method with Molecular Volume (GBMV). To obtain the relative structural stability of the Aβ_{1-42} oligomers, the Aβ trajectories of the last 5 ns were first extracted from the explicit MD simulation excluding water molecules. The solvation energies of all systems were calculated using the GBMV (16, 17). In the GBMV calculations, the dielectric constant of water was set to 80.0. The hydrophobic solvent-accessible surface area (SASA) term factor was set to 0.00592 kcal/mol · Å^2. Each conformer is minimized 1,000 cycles, and the conformation energy is evaluated by grid-based GBMV. The minimization does not change the conformations of each conformer, but only relaxed the local geometries due to thermal fluctuation that occurred during the MD simulations.

A total of 10,000 conformations (500 conformations for each of the 20 conformers examined) were used to construct the effective energy landscape of the Aβ_{1-42} oligomer and to evaluate the conformer probabilities by using Monte Carlo (MC) simulations. At the first step one conformation of conformer i and one conformation of conformer j are randomly selected. Then, the Boltzmann factor is computed as $e^{-(E_j-E_i)/KT}$, where E_i and E_j are the conformational energies evaluated using the GBMV calculations for the conformation i and j, respectively, K is the Boltzmann constant, and T is the absolute temperature (298 K used here). If the Boltzmann factor value is larger than the random number, the move from conformation i to conformation j is allowed. After 1 million steps, the conformations visited for each conformer were counted. Finally, the relative probability of conformer n was evaluated as $P_n = N_n/N_{\text{total}}$, where P_n is the population of conformer n, N_n is the total number of conformations visited for the conformer n, and N_{total} is the total steps. The advantages of using the MC simulations to estimate conformer probability rely on the facts that the MC simulations have good numerical stability and allow transition probabilities among several conformers to be controlled (18). The populations of the conformers are only indicative.

Analysis Details. We also examined the structural stability of the Aβ_{42} oligomeric *tubular* $M1_1$, $M1_2$, and $M1_3$ variants by following the backbone-backbone distance of Cα of G27 to the two C atoms of F4. These distances were calculated and then averaged. We further examined the stability of the oligomers $M1_1$, $M1_2$, and $M1_3$by following changes in the number of hydrogen bonds between the β-sheets with the hydrogen bond cutoff set to 2.5 Å. Finally, the E11-E11 and E22-E22 distances between two opposite peptides in the each *tubular* model were averaged. Three layers at each end of the fibril-like of models $M1_1$, $M1_2$, and $M1_3$ were excluded in the analysis.

β-Sheet Structure Along the N-Terminal. The role of the N-terminal in the stability of the structures studied here is crucial. We computed the percentage of the β-sheet structure along the N-terminal of all peptides for model M1 (the model that fits the experimental cryoEM) at the various pH values. Fig. S10*B* illustrates that at pH = 5–6, residues R5-Y10 in the N-terminal form β-sheet; and at physiological pH and at very acidic pH (pH = 3–4) residues F4-Y10 in the N-terminal form β-sheet. The results indicate that β-sheet structures along the N-terminal assist in stabilizing the fibril.

1. Zhang R, et al. (2009) Interprotofilament interactions between Alzheimer's Abeta1-42 peptides in amyloid fibrils revealed by cryoEM. *Proc Natl Acad Sci USA* 106:4653–4658.
2. Lührs T, et al. (2005) 3D structure of Alzheimer's amyloid-beta(1-42) fibrils. *Proc Natl Acad Sci USA* 102:17342–17347.
3. Petkova AT, Yau WM, Tycko R (2006) Experimental constraints on quaternary structure in Alzheimer's beta-amyloid fibrils. *Biochemistry* 45:498–512.
4. Kale L, et al. (1999) NAMD2: Greater scalability for parallel molecular dynamics. *J Comput Phys* 151:283–312.
5. MacKerell AD, et al. (1998) All-atom empirical potential for molecular modeling and dynamics studies of proteins. *J Phys Chem B* 102:3586–3616.
6. Brooks BR, et al. (1983) Charmm—a program for macromolecular energy, minimization, and dynamics calculations. *J Comput Chem* 4:187–217.
7. Mahoney MW, Jorgensen WL (2000) A five-site model for liquid water and the reproduction of the density anomaly by rigid, nonpolarizable potential functions. *J Chem Phys* 112:8910–8922.
8. Jorgensen WL, Chandrasekhar J, Madura JD, Impey RW, Klein ML (1983) Comparison of simple potential functions for simulating liquid water. *J Chem Phys* 79:926–935.
9. Martyna GJ, Tobias DJ, Klein ML (1994) Constant-pressure molecular-dynamics algorithms. *J Chem Phys* 101:4177–4189.
10. Feller SE, Zhang YH, Pastor RW, Brooks BR (1995) Constant-pressure molecular-dynamics simulation—the Langevin piston method. *J Chem Phys* 103:4613–4621.
11. Darden T, York D, Pedersen L (1993) Particle mesh Ewald—An N.Log(N) method for Ewald sums in large systems. *J Chem Phys* 98:10089–10092.
12. Essmann U, et al. (1995) A smooth particle mesh Ewald method. *J Chem Phys* 103:8577–8593.
13. Ryckaert JP, Ciccotti G, Berendsen HJC (1977) Numerical-integration of Cartesian equations of motion of a system with constraints—molecular-dynamics of N-alkanes. *J Comput Phys* 23:327–341.
14. Chacon P, Wriggers W (2002) Multi-resolution contour-based fitting of macromolecular structures. *J Mol Biol* 317:375–384.
15. Lewiner T, Lopes H, Vieira A, Tavares G (2003) Efficient implementation of marching cubes' cases with topological guarantees. *J Graph Tools* 8:1–16.
16. Lee MS, Salsbury FR, Brooks CL (2002) Novel generalized Born methods. *J Chem Phys* 116:10606–10614.
17. Lee M S, Feig M, Salsbury FR, Brooks CL (2003) New analytic approximation to the standard molecular volume definition and its application to generalized born calculations. *J Comput Chem* 24:1348–1356.
18. Ma B, Levin AJ (2007) Probing potential binding modes of the p53 tetramer to DNA based on the symmetries encoded in p53 response elements. *Nucl. Acids Res.* 35:7733–7747.

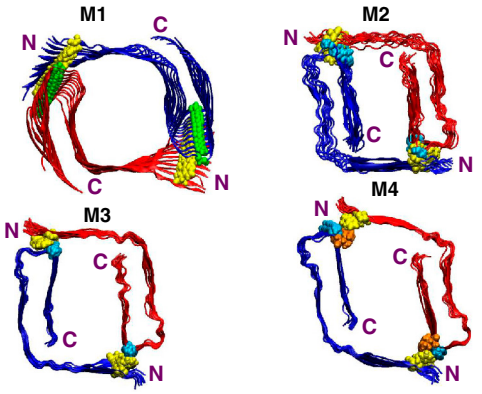

Fig. S1. The initial constructed models M1, M2, M3, and M4 based on Lührs model (PDB ID code 2BEG) (ref. 4) are illustrated. All models demonstrate intermolecular hydrophobic interactions between the N-termini of one oligomer and the loop region of the second oligomer: Phe, yellow; Gly, green; Ala, blue; and Ile, orange. The C-termini of these models face the internal surface of the fibril.

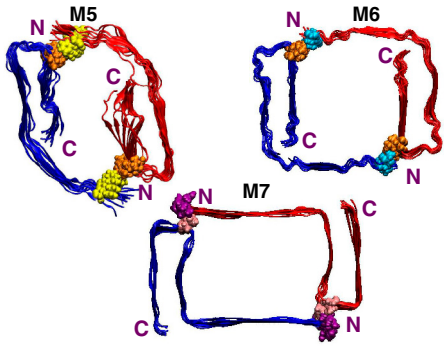

Fig. S2. The initial constructed models M5, M6, and M7 based on Lührs model (PDB ID code 2BEG) (ref. 4) are illustrated. Models M5 and M6 demonstrate intermolecular hydrophobic interactions between the N-termini of one oligomer and the loop region of the second oligomer, whereas model M7 demonstrates charge-charge interactions: Phe, yellow; Ala, blue; Ile, orange; Asp, purple; and Asn, pink. The C-termini of models M5 and M6 face the internal surface of the fibril, whereas in model M7 they face the external surface of the fibril.

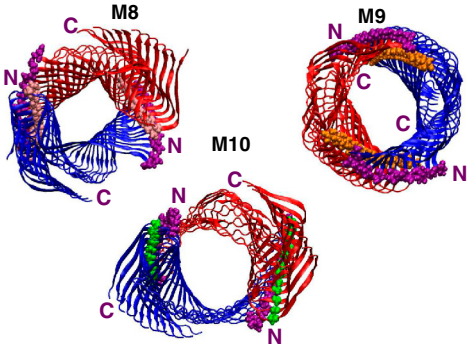

Fig. S3. The initial constructed models M8, M9, and M10 based on Lührs model (PDB ID code 2BEG) (ref. 4) are illustrated. Model M8 demonstrates intermolecular hydrophobic interactions between the N-termini of one oligomer and the loop region of the second oligomer, whereas models M9 and M10 show side-chain interactions: Gly, green; Ile, orange; Asp, purple; and Asn, pink. In all models the monomers were initially rotated by 10° along the fibril axis. The C-termini of models M8 and M10 face the internal surface of the fibril, whereas in model M9 they face the internal surface of the fibril.

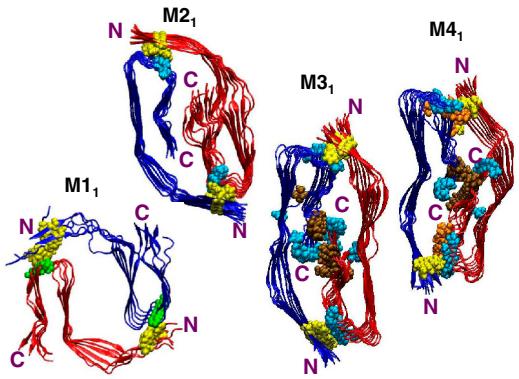

Fig. S4. Final snapshot from simulations of 60 ns for models $M1_1$, $M2_1$, $M3_1$, and $M4_1$ at pH = 7: $M1_1$ exhibits N-term-loop interactions between F4 (yellow) and G29 (green); only six interior layers of each oligomer are presented here. $M2_1$ exhibits N-term-loop interactions between F4 (yellow) and A30 (blue). $M3_1$ shows both N-term-loop interactions between F4 (yellow) and A30 (blue) and hydrophobic core interaction between V39 (brown) and A42 (blue). $M4_1$ presents similar interactions as $M3_1$, but includes also F4 (yellow)-I31 (orange) interactions in the N-term-loop domain.

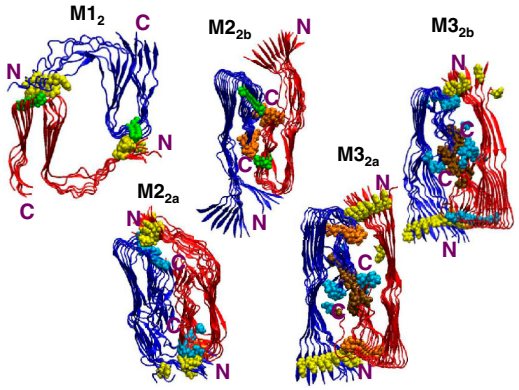

Fig. S5. Final snapshot from simulations of 60 ns for models $M1_2$, $M2_{2a}$, $M2_{2b}$, $M3_{2a}$, and $M3_{2b}$ at pH = 5–6: $M1_2$ exhibits N-term-loop interactions between F4 (yellow) and G29 (green); only six interior layers of each oligomer are presented here. $M2_{2a}$ exhibits N-term-loop interactions between F4 (yellow) and A30 (blue). $M2_{2b}$ shows hydrophobic core interaction between G29 (green) and I41 (orange). $M3_{2a}$ presents hydrophobic core interaction between V39 (brown) and A42 (blue) and N-term-loop interactions between F4 (yellow) and I41 (orange). $M3_{2b}$ demonstrates N-term-loop interactions between F4 (yellow) and A30 (blue) and hydrophobic core interaction between V39 (brown) and A42 (blue).

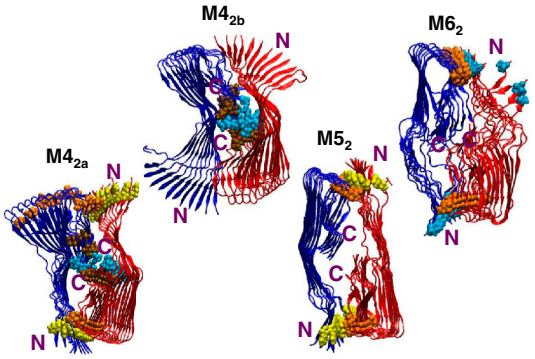

Fig. S6. Final snapshot from simulations of 60 ns for models $M4_{2a}$, $M4_{2b}$, $M5_2$, and $M6_2$ at pH = 5–6: $M4_{2a}$ demonstrates N-term-loop interactions between F4 (yellow) and I41 (orange) and hydrophobic core interaction between V39 (brown) and A42 (blue). $M4_{2b}$ shows hydrophobic core interaction between V39 (brown) and A42 (blue). $M5_2$ presents N-term-loop interactions between F4 (yellow) and I41 (orange). $M6_2$ shows N-term-loop interactions between A2 (blue) and I41 (orange).

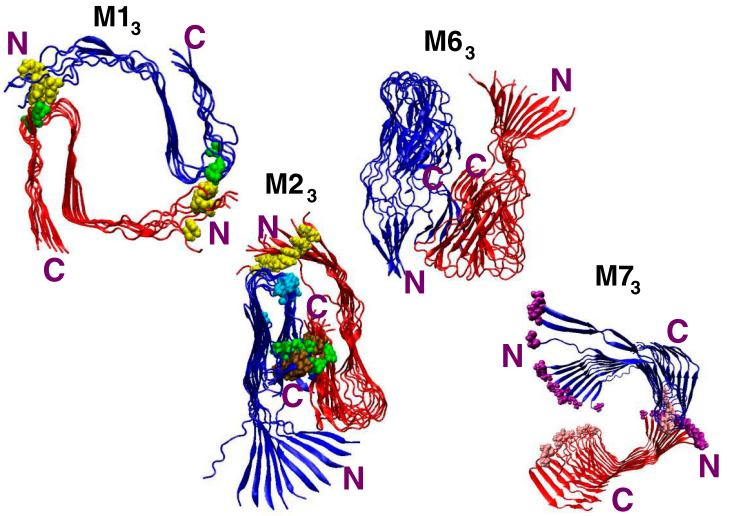

Fig. S7. Final snapshot from simulations of 60 ns for models $M1_3$, $M2_3$, $M6_3$, and $M7_3$ at pH = 3–4: $M1_3$ exhibits N-term-loop interactions between F4 (yellow) and G29 (green); only six interior layers of each oligomer are presented here. $M1_2$ exhibits N-term-loop interactions between F4 (yellow) and A30 (blue) and hydrophobic core interaction between V39 (brown) and G29 (green). $M6_3$ does not exhibit any interaction between the two oligomers. $M7_3$ demonstrates N-term-loop interactions only in one side between D1 (purple) and N27 (pink).

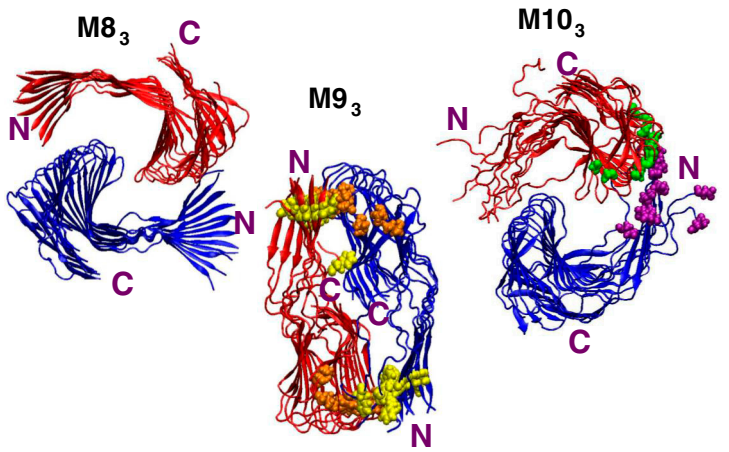

Fig. S8. Final snapshot from simulations of 60 ns for models $M8_3$, $M9_3$, and $M10_3$ at pH = 3–4: $M8_3$ does not exhibit any interaction between the two oligomers. $M9_3$ demonstrates N-term-loop interactions between F4 (yellow) and I41 (orange). $M10_3$ shows N-term-loop interactions only on one side between D1 (purple) and G29 (green).

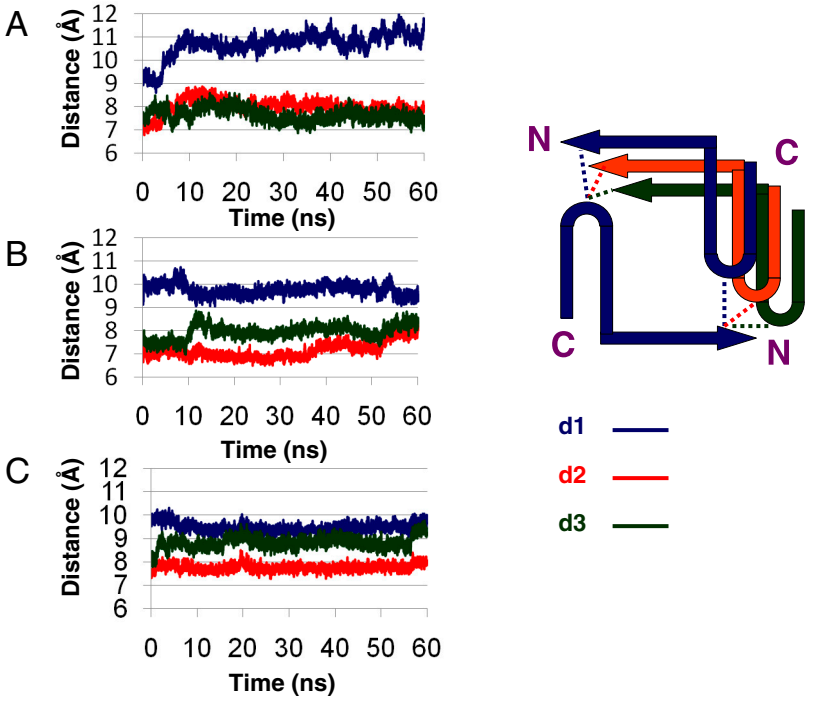

Fig. S9. Structural similarity of models derived from model M1 at different pH values is demonstrated. Three different F4-G29 distances are illustrated for (*A*) model $M1_1$ at pH = 7, (*B*) model $M1_2$ at pH = 5–6, and (*C*) model $M1_3$ at pH = 3–4, along the simulations: First distance is between N-termini and loop regions at the same plane of the initial structural model (blue line). Second distance is between N-termini of one plane and loop regions, in a cross-first sequential plane (red line). Third distance is between N-termini of one plane and loop regions, in a cross-second layer plane (green line). Three layers at each end of the fibril-like of models $M1_1$, $M1_2$, and $M1_3$ were excluded for analysis.

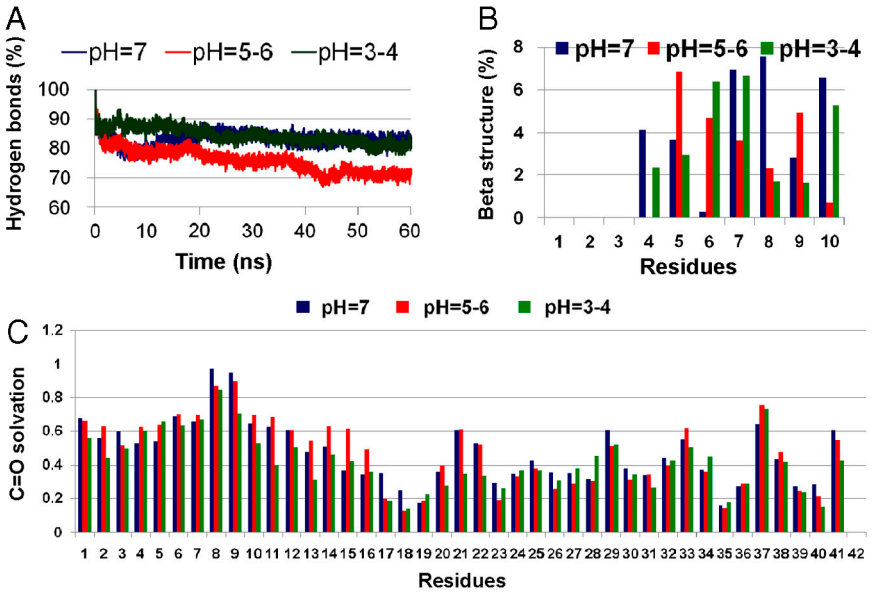

Fig. S10. (*A*) The fraction of the number of hydrogen bonds (in percentage) between β-sheets for model M11 at pH = 7 (blue line), model M12 at pH = 5–6 (red line), and for M13 at pK = 3–4 (green line). Three layers at each end of the fibril-like of models M11, M12, and M13 were excluded for analysis. (*B*) The averaged percentage of the beta sheet structure of residues D1-Y10 in the N-terminal for model M11 at pH = 7 (blue), model M12 at pH = 5–6 (red), and for M13 at pK = 3–4 (green). (*C*) The backbone solvation (C=O solvation in the Y-axis) for residues D1-A42 for model $M1_1$ at pH = 7 (blue), model $M1_2$ at pH = 5–6 (red), and for $M1_3$ at pK = 3–4 (green).

Table S1. The 10 tubular constructed models M1–M10

Model	C-termini face*	N-termini-loop regions' interactions†	Rotated angle along its fibril growth axis	Figure
M1	O	F4, G29	5	1, S1
M2	I	F4, A30	—	S1
M3	I	F4, A30	—	S1
M4	I	F4, A30, I31	—	S1
M5	I	F4, I31	—	S2
M6	I	A2, I31	—	S2
M7	O	D1, N27	—	S2
M8	O	D1, N27	10	S3
M9	I	D1, I31	10	S3
M10	O	D1, G29	10	S3

*For *tubular* models, two possibilities exist for the C-termini arrangement: one with the C termini of each Aβ monomer facing the external surface of the fibril (O) and the second when it faces the internal of the fibril cavity (I).

†Models M1–M6 present hydrophobic interactions between the N termini and the loop regions, M7 and M8 demonstrate charge–charge interactions, and M9 and M10 show side chain interactions.

Table S2. The 20 simulated models at different pH values, derived from the tubular constructed models M1–M10, and the geometrical constraints

Model	pH value	Derived from model	Total time of geometrical constraints, ns	Geometrical constraints between hydrogen bonds of residues
$M1_1$	7	M1	1	17–42
$M2_1$	7	M2	5	1–42
$M3_1$	7	M3	5	1–42
$M4_1$	7	M4	5	1–42
$M1_2$	5–6	M1	1	17–42
$M2_{2a}$	5–6	M2	1	1–42
$M2_{2b}$	5–6	M2	5	1–42
$M3_{2a}$	5–6	M3	1	1–42
$M3_{2b}$	5–6	M3	5	1–42
$M4_{2a}$	5–6	M4	1	1–42
$M4_{2b}$	5–6	M4	5	1–42
$M5_2$	5–6	M5	5	1–42
$M6_2$	5–6	M6	5	1–42
$M1_3$	3–4	M1	1	17–42
$M2_3$	3–4	M2	1	1–42
$M6_3$	3–4	M6	1	1–42
$M7_3$	3–4	M7	1	1–42
$M8_3$	3–4	M8	1	1–42
$M9_3$	3–4	M9	1	1–42
$M10_3$	3–4	M10	1	17–42